SUPPLEMENTAL APPENDIX

Corrections for Partial-Volume, Delay and Dispersion

The apparent activity in the left ventricle (LV) deviates from the 'true' activity due to partial-volume effect caused by limited spatial resolution, cardiac and respiratory motion. Moreover, the blood and plasma time-activity curves (TACs) differ from their 'true' measurements at the organ/tissue due to limited sampling rate, time delay, and dispersion associated with the manual blood sampling technique. In this study, the femoral blood samples ($C_B(t)$) obtained within 1-min after tail vein intravenous (IV) ^{18}F-FDG injection was assumed to be equal to the LV TAC ($C_{LV}(t)$) corrected for partial-volume averaging, shifted in time, and dispersed by a single-exponential kernel (*1*,*2*), according to the following equation:

$$C_B(t) = \frac{C_{LV}(t-\Delta)}{RC} \otimes \frac{e^{-(t-\Delta)/\tau}}{\tau} \quad \text{for } 0 \le t < 1 \text{ min} \qquad \text{Eq. 1}$$

where RC represents the recovery coefficient for correction of partial-volume effect on the LV TAC; $\triangle$ (min) and τ (min) represent, respectively, the delay and dispersion time constants for the tracer to transit from the LV chamber to the femoral artery catheter, where blood samples are taken; and $\otimes$ denotes the mathematical operation of convolution. The myocardial activity is assumed to be much lower than that in the LV within 1 min post-injection so that its spillover of activity to the LV chamber is negligible. The above formulation is similar to the compartmental modeling approach previously proposed by our group (*3*), except that the delay ($\triangle$) and the dispersion (τ) parameters are now separately modeled. The parameters $\triangle$, τ and RC can be simultaneously estimated by nonlinear least-squares fitting the measured $C_B(t)$ to Eq. 1.

Whole Blood and Plasma Input Function

The organ or tissue of interest was assumed to be approximately halfway between the LV and the femoral artery catheter and hence, the time delay and dispersion time constants can be approximated by half of the fitted values of $\triangle$ and τ for the tissue of interest (*3*). Thus for IV injection studies, the complete time course of arterial blood in tissue ($C_W(t)$) had a better temporal resolution around the peak composed of a concatenation of partial-volume, delay, and dispersion corrected early-time LV data (t < 1 min) and the serial femoral blood sample measurements ($t \ge 1$ min):

$$C_W(t) = \begin{cases} \dfrac{C_{LV}(t-\Delta/2)}{RC} \otimes \dfrac{e^{-2(t-\Delta/2)/\tau}}{\tau/2}, & 0 \le t < 1 \text{ min} \\ \text{femoral blood samples}, & t \ge 1 \text{ min} \end{cases} \quad \text{Eq. 2}$$

The plasma input function ($C_P(t)$) was constructed by multiplying the early portion (t < 1 min) of $C_W(t)$ by the plasma-to-whole blood ratio ($R_{PB}(t)$) to correct for the ^{18}F-FDG uptake by RBC and concatenating with the manually drawn plasma samples ($t \ge 1$ min). For intraperitoneal (IP) ^{18}F-FDG injection studies, manually drawn samples were used directly to form the whole-blood TAC and plasma input function.

REFERENCE

1. Iida H, Higano S, Tomura N, et al. Evaluation of regional differences of tracer appearance time in cerebral tissues using [^{15}O]water and dynamic positron emission tomography. *J Cereb Blood Flow Metab.* 1988;8:285-288.

2. Herrero P, Hartman JJ, Senneff MJ, Bergmann SR. Effects of time discrepancies between input and myocardial time-activity curves on estimates of regional myocardial perfusion with PET. *J Nucl Med.* 1994;35:558-566.

3. Ferl GZ, Zhang X, Wu H-M, Huang S-C. Estimation of the ^{18}F-FDG input function in mice by use of dynamic small-animal PET and minimal blood sample data. *J Nucl Med.* 2007;48:2037-2045.

SUPPLEMENTAL TABLE

SUPPLEMENTAL TABLE 1: Parameter estimates for the plasma-to-whole blood ratio, $R_{PB}(t)$, obtained for IV and IP injection studies under nonfasting and fasting conditions.

	IV		IP	
Parameter	Nonfasted (n = 6)	Fasted (n = 5)	Nonfasted (n = 6)	Fasted (n = 6)
A (unitless)	0.369 ± 0.136	0.432 ± 0.087[*]	0.667 ± 0.345	0.814 ± 0.210[*]
β (min^{-1})	0.066 ± 0.016[†]	0.168 ± 0.044[*†]	0.118 ± 0.082	0.087 ± 0.041[*]
ρ (unitless)	1.081 ± 0.067	1.158 ± 0.052	1.112 ± 0.109	1.086 ± 0.065

Values are mean ± SD.
[*] $P < 0.05$
[†] $P < 0.01$

SUPPLEMENTAL FIGURES

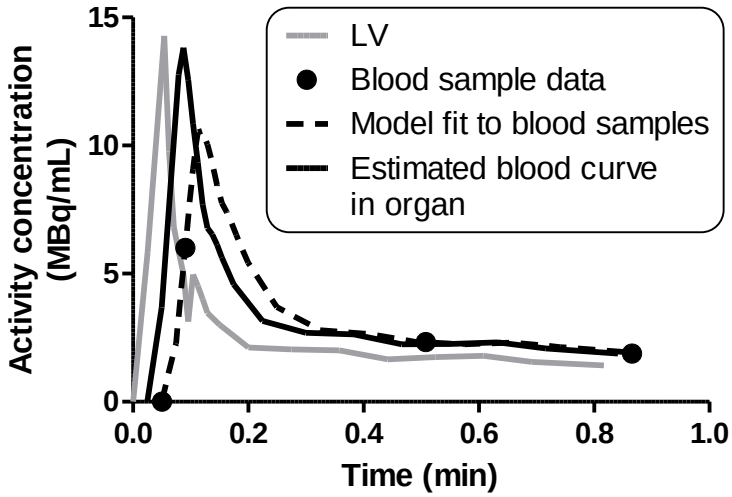

SUPPLEMENTAL FIGURE 1: Partial-volume, delay and dispersion corrections of left ventricle (LV) time-activity curve in an IV injection study.

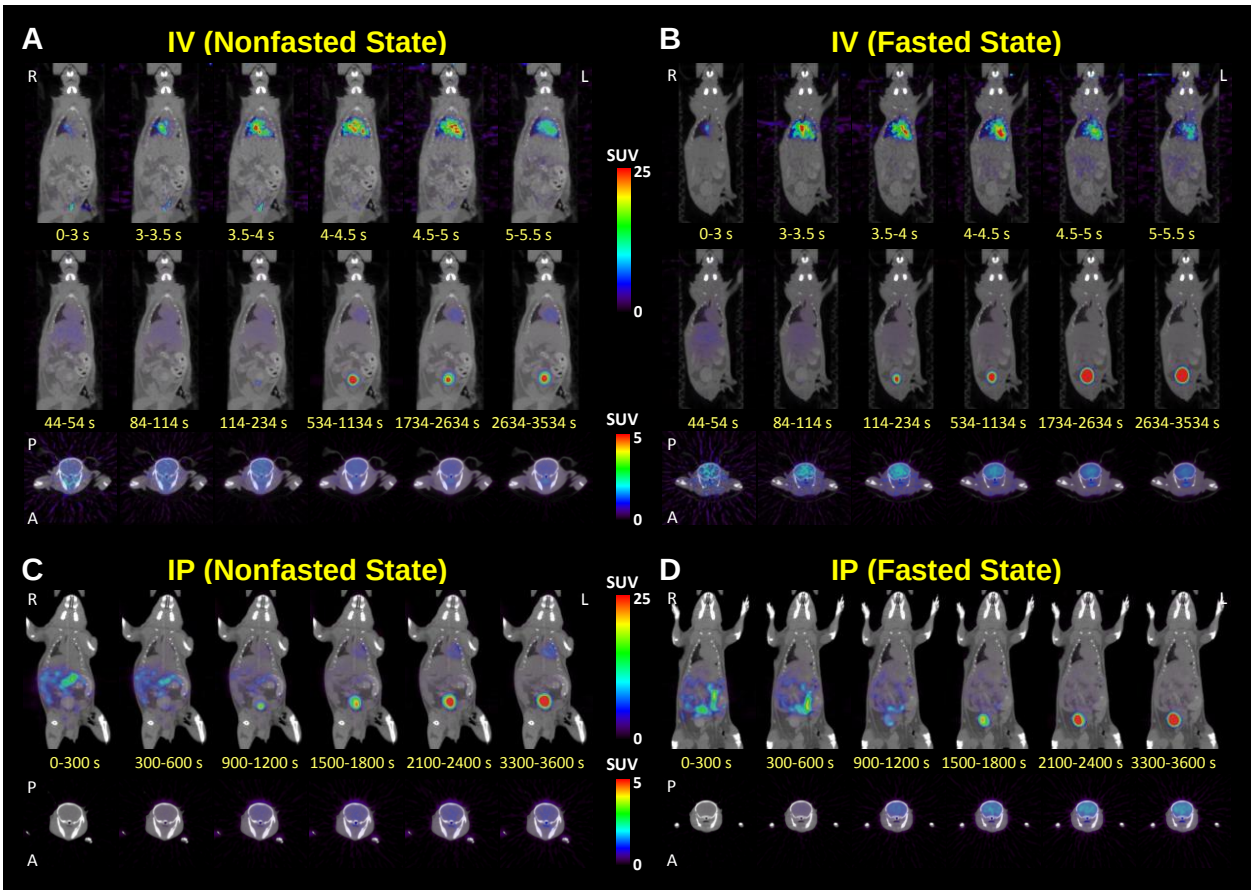

SUPPLEMENTAL FIGURE 2: Representative examples of biodistribution of ^{18}F-FDG at different times after injection in (A) nonfasted IV, (B) fasted IV, (C) nonfasted IP, and (D) fasted IP injection studies. Small-animal PET images are fused with CT images for anatomic localization of structures such as myocardium, lung, liver, gastrointestinal tract, and urinary bladder (shown in coronal view) and brain (shown in transaxial view). Color bars are scaled differently for coronal and transaxial views.

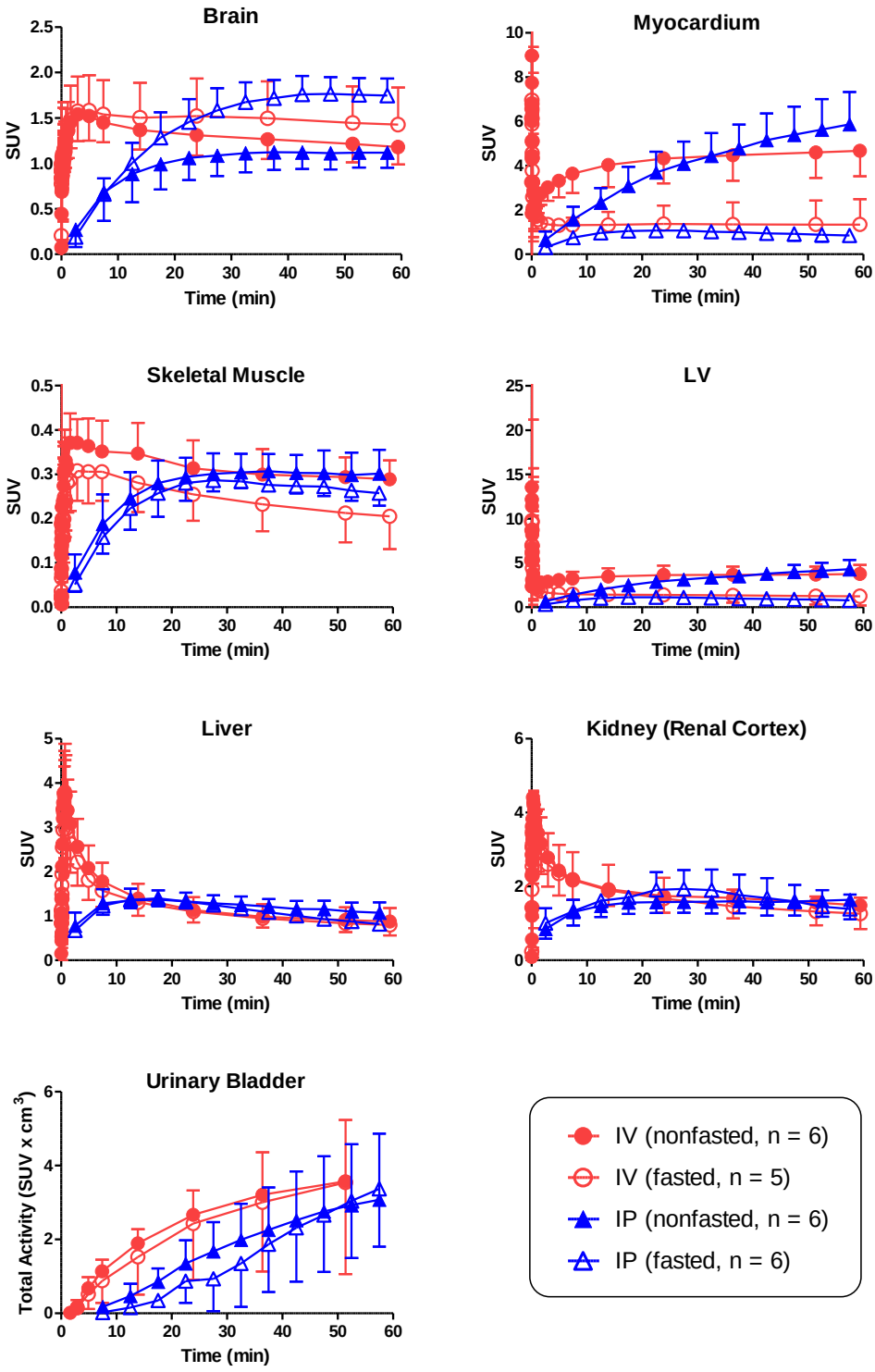

SUPPLEMENTAL FIGURE 3: Mean time-activity curves of the brain, myocardium, skeletal muscle, left ventricle (LV), liver, kidney (renal cortex), and total activity in urinary bladder. Error bars represent 1 SD.

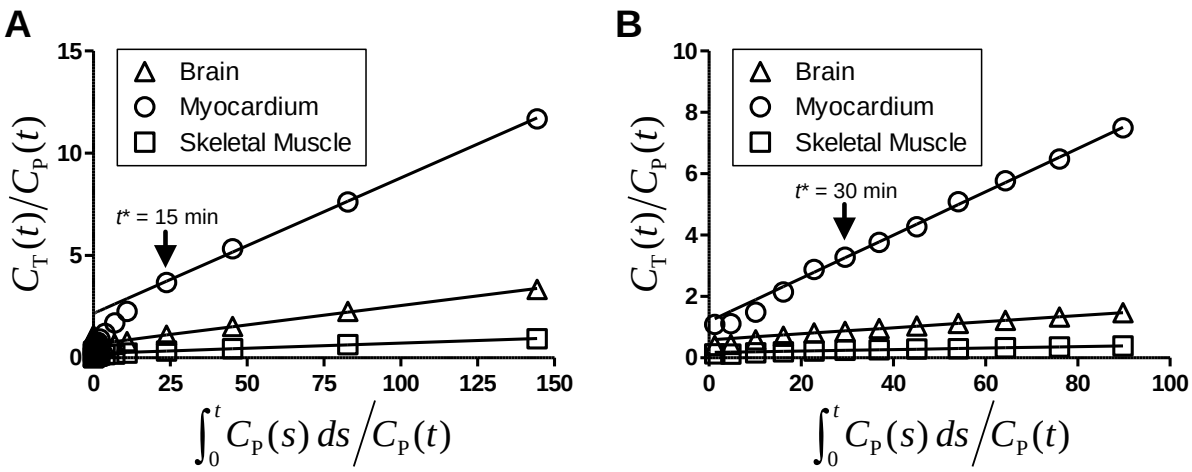

SUPPLEMENTAL FIGURE 4: Patlak plots of the brain, myocardium and skeletal muscle for (A) IV and (B) IP injection studies. The time point (t^*) after which the Patlak plots become linear is indicated for IV and IP injection studies.

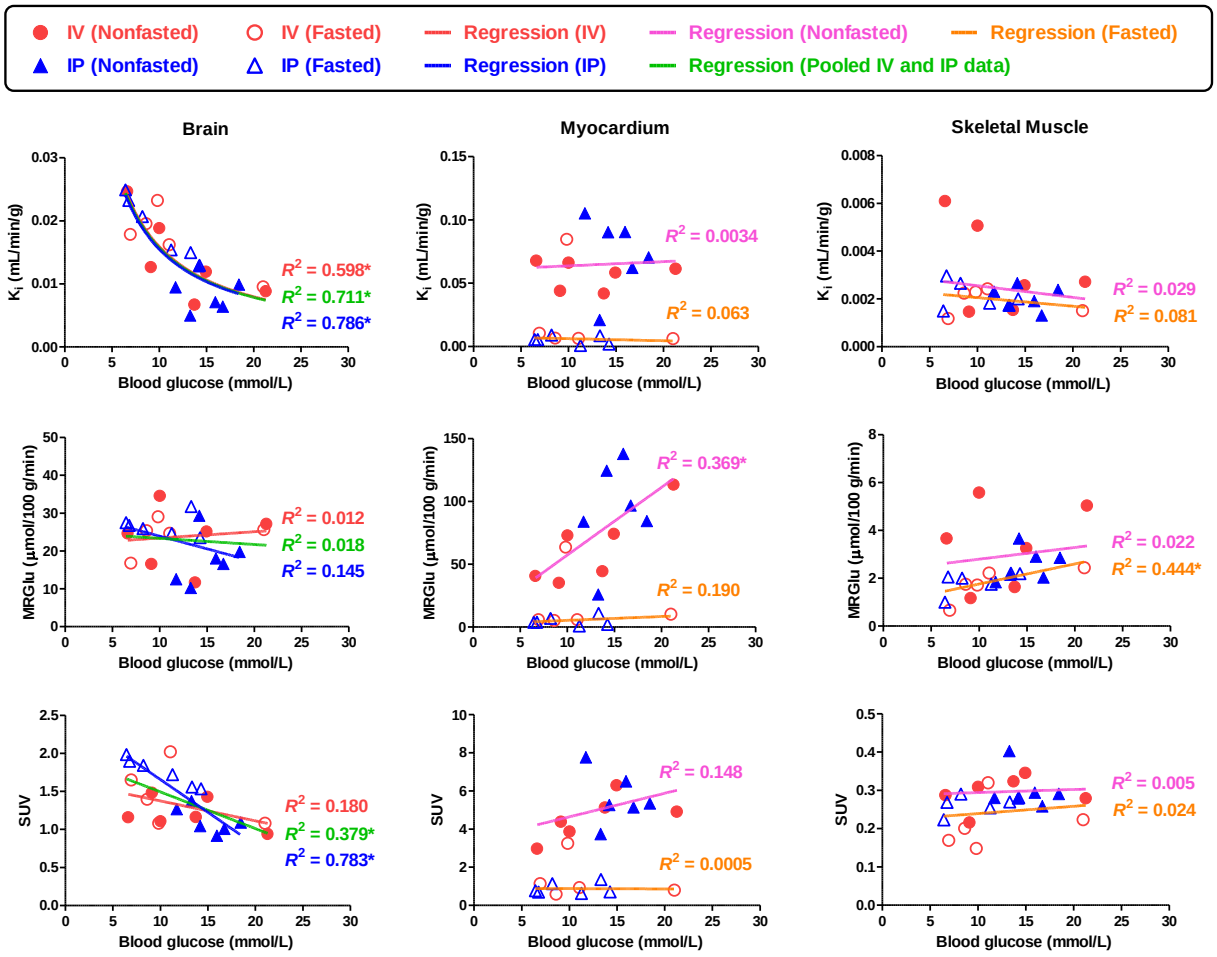

SUPPLEMENTAL FIGURE 5: Relationships between blood glucose levels and ^{18}F-FDG uptake constant (K_i), metabolic rate of glucose (MRGlu), and standardized uptake value (SUV) in the brain, myocardium, and skeletal muscle. *Regression is strongly significant at $P < 0.05$.